

1 **Thermodynamics and Kinetics of Refractory Multi-Principal Element Alloys: An**  
2 **Experimental and Modeling Comparison**

3  
4 R. Puerling<sup>1</sup>, A. Miklas<sup>1</sup>, F.G. Coury<sup>1,2</sup>, N.R. Philips<sup>3</sup>, P. Mason<sup>4</sup>, N.E. Peterson<sup>1\*</sup>, A. Deal<sup>5</sup>, J.  
5 Klemm-Toole<sup>1</sup>, A.J. Clarke<sup>1</sup>

6  
7 <sup>1</sup>Colorado School of Mines, Golden, CO 80401

8 <sup>2</sup>Universidade Federal de São Carlos, São Carlos – SP, 13565-905, Brazil

9 <sup>3</sup>Allegheny Technologies Incorporated, Albany, OR 97321

10 <sup>4</sup>Thermo-Calc Software, McMurray, PA 15317

11 <sup>5</sup>Kansas City National Security Campus, Kansas City, MO 64147

12  
13 \*nepeterson@mines.edu

14  
15  
16 The search for structural alloys capable of ultrahigh temperature performance has led to the  
17 exploration of refractory multi-principal element alloys (RMPEAs). In this work, experimental  
18 results for solidification segregation and homogenization of two RMPEAs, NbTaTiW and  
19 MoNbTaTi, are compared to simulations using the Scheil and DICTRA modules in Thermo-  
20 Calc®. Scheil calculations accurately predict the observed solidification segregation, while  
21 DICTRA predicts general trends and can provide a minimum time to achieve homogenization at  
22 a given temperature.

23  
24 As technological advances reach their limits with currently available materials, advanced  
25 structural metallic alloys need to be discovered and developed for multiple key areas, including  
26 ultrahigh temperature performance in extreme environments. High-entropy alloys (HEAs), also  
27 referred to as multi-principal element alloys (MPEAs) or complex concentrated alloys (CCAs),  
28 have become a popular area of research during the last 15 years because they offer potential  
29 property combinations otherwise unattainable with conventional alloys. [1] The need for metallic  
30 structural alloys for use in ultrahigh temperature applications has led to the exploration of  
31 MPEAs comprised of only, or primarily, refractory metals. These alloys are known as refractory  
32 multi-principal element alloys (RMPEAs).

33 Although RMPEAs are capable of maintaining high strengths at elevated temperatures, their  
34 fabrication is generally limited by room and low temperature ductility, especially in the as-cast  
35 condition, making thermomechanical processing challenging. [1–10] The use of thermodynamic  
36 simulation programs, such as Thermo-Calc®, has been demonstrated as useful tools for screening

37 of potential compositions in alloy design studies in a wide variety of alloy systems, including  
38 steels [11–13], aluminum [14,15], Ni-based alloys [16], and MPEAs [4,17,18]. This work  
39 compares experimental data with predictions of the solidification and homogenization behavior  
40 of the equimolar RMPEAs NbTaTiW and MoNbTaTi using Thermo-Calc®.

41 The Scheil-Gulliver model [19,20] and DICTRA module [21] available in Thermo-Calc®  
42 (Version 2021a) were used to simulate spatial variations in composition during solidification and  
43 homogenization, respectively, of the NbTaTiW and MoNbTaTi alloys. For the simulations, the  
44 TCHEA4 and MOBHEA2 databases were used to provide the thermodynamic and mobility data,  
45 respectively. The initial segregation results obtained from Scheil-Gulliver simulations were  
46 subsequently used to initialize the homogenization simulations. To explore the effects of the  
47 solidification microstructure on the homogenization kinetics, homogenization simulations were  
48 run with effective secondary dendrite arm spacings of 1000, 100, and 10  $\mu\text{m}$ . The parameter used  
49 in Thermo-Calc® to capture secondary dendrite arm spacing is length scale. These were chosen  
50 to see the difference the order of magnitude makes on the simulations. Length scale is the  
51 distance over which segregation can be observed and is representative of the distance from the  
52 center of a secondary dendrite arm to the center of the interdendritic region adjacent to it and is  
53 therefore proportional to the secondary dendrite arm spacing. The simulated homogenization  
54 treatment was 35 hours at 1673K.

55  
56 The measured compositions of the NbTaTiW and MoNbTaTi alloys investigated in this work are  
57 shown in Table 1. The alloys listed in Table 1 were produced by Allegheny Technologies  
58 Incorporated, in collaboration with the Center for Advanced Non-Ferrous Structural Alloys at the  
59 Colorado School of Mines. Additional details regarding sample preparation are provided in  
60 [8,10]. These alloys were made by non-consumable arc melting of high quality, remelt grade  
61 elements in an inert argon atmosphere. Each button was re-melted three times to achieve a well-  
62 mixed sample.

63 Table 1: Bulk compositions (at %) for the RMPEAs NbTaTiW and MoNbTaTi measured by  
64 EDS.

65

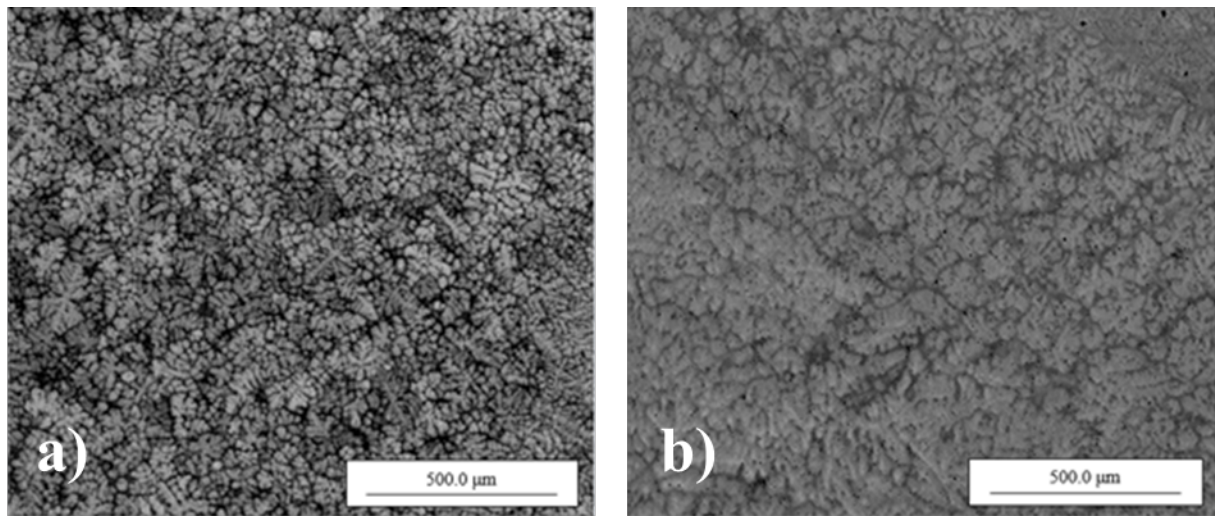
	<b>Mo/W</b>	<b>Nb</b>	<b>Ta</b>	<b>Ti</b>
<b>MoNbTaTi</b>	25.3	24.6	24.8	25.3
<b>NbTaTiW</b>	26.4	24.5	24.5	24.6

66  
67 The alloy buttons were then heat treated under vacuum at 1673K for 35 h in an attempt to  
68 achieve homogenization. Samples in both the as-cast and heat-treated condition were ground to a  
69 1200 grit surface finish with different SiC metallographic papers, followed by polishing with 6  
70  $\mu\text{m}$ , 3  $\mu\text{m}$ , and 1  $\mu\text{m}$  diamond media for about 5 min each. A final polishing step of 0.05  $\mu\text{m}$   
71 colloidal silica was performed for a total of 8 h in a vibratory polisher. The samples were then  
72 imaged and characterized using Scanning Electron Microscopy (SEM) using an FEI Quanta 600i  
73 Environmental SEM equipped with an Energy Dispersive X-Ray Spectroscopy (EDS) detector  
74 (EDAX Element). For the compositional measurements using EDS, the count time per pixel was  
75 set to 100 s and the accelerating voltage was set to 25 kV. [22] The raw counts obtained for each  
76 EDS spectra were subsequently converted to atomic fractions using the vendor supplied ZAF  
77 correction scheme (EDAX Team software).

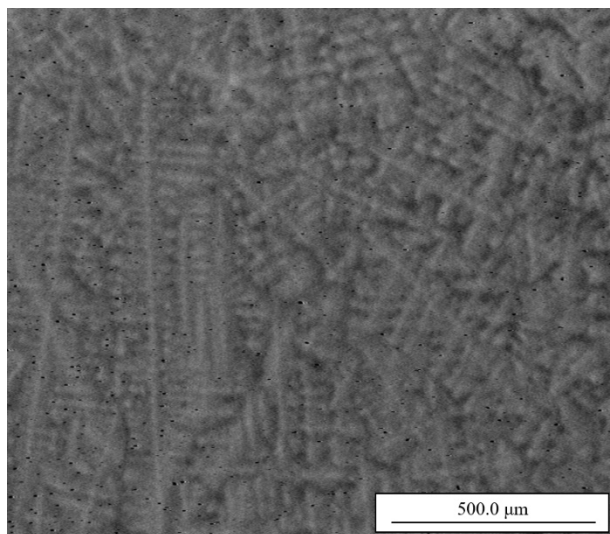
78  
79 The solidification segregation behavior prior to homogenization heat treatment has been  
80 evaluated experimentally for similar alloys. Samples of NbTaV-(Ti, W) and MoNbTaV were  
81 made by arc melting commercially pure elemental powder, each button being re-melted three  
82 times. The NbTaV-(Ti, W) samples were observed to have Ta and W-rich dendrite cores and Nb,  
83 Ti, and V-rich interdendritic regions. [23] In the MoNbTaV sample, the dendrite cores were  
84 observed to be Ta-rich, while the interdendritic regions were found to be Nb, Mo, and V-rich.  
85 [24] Therefore, in the MoNbTaTi, it is expected that the dendrite cores will be Ta-rich and the  
86 interdendritic regions will be Mo, Nb, and Ti-rich, while in the NbTaTiW, it is expected that the  
87 dendrite cores will be Ta and W-rich, and the interdendritic regions will be Nb and Ti-rich.

88  
89 Back-scattered electron (BSE) micrographs of the as-cast and heat-treated (35 hours at 1673K)  
90 of the NbTaTiW alloy are shown in Figure 1. The dendritic structure in the as-cast condition,  
91 shown in Figure 1(a) indicates a secondary dendrite arm spacing of 10-30  $\mu\text{m}$ . Secondary  
92 dendrite arm spacing was evaluated by taking 20 measurements from the center of different  
93 secondary dendrite arms to the center of their adjacent interdendritic regions. SEM BSE  
94 micrographs after homogenization at 1673K for 35 h also reveal contrast associated with residual  
95 compositional segregation, as shown in Figure 1(b). Figure 2 also shows similar residual

96 compositional segregation from solidification in MoNbTaTi after homogenization at 1673K for  
97 35 h.

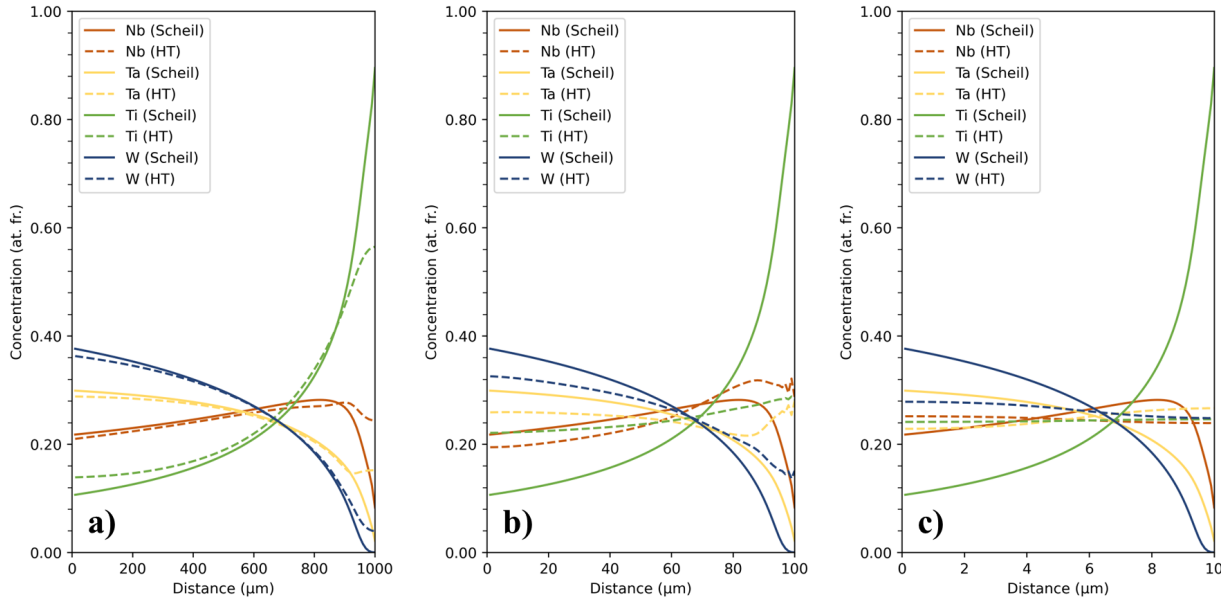


98  
99  
100 Figure 1: SEM BSE micrographs of (a) as-cast and (b) heat treated (1673K for 35 h) NbTaTiW.  
101

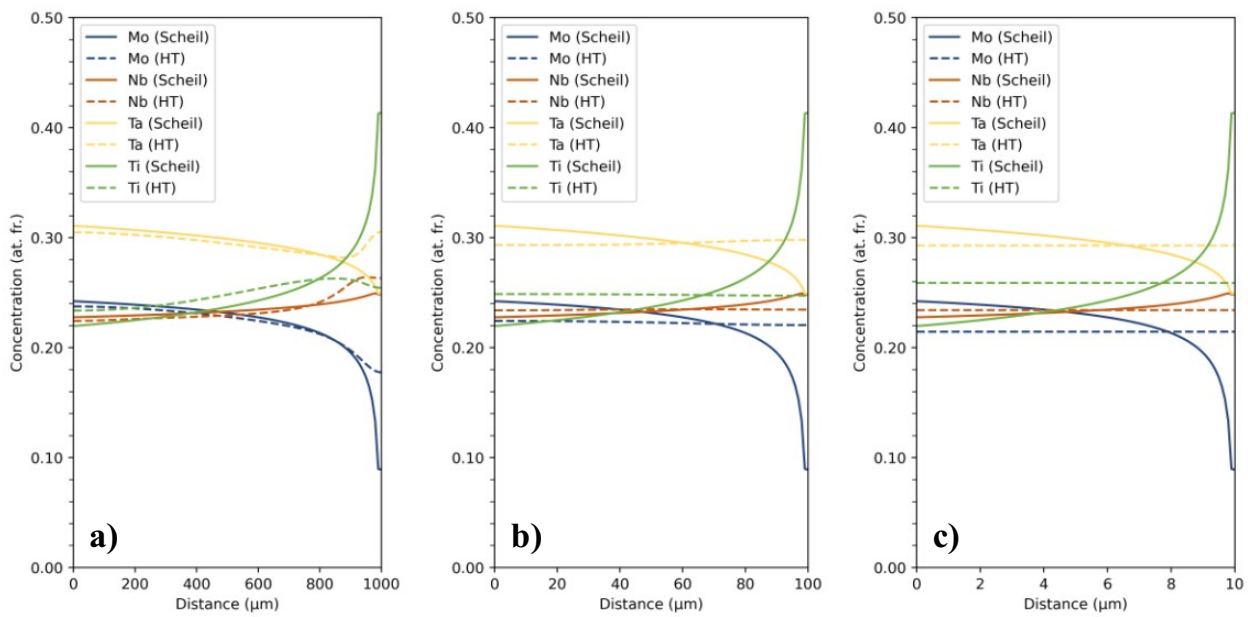


102  
103  
104 Figure 2: SEM BSE micrograph of MoNbTaTi after heat treatment at 1673K for 35 h.  
105  
106 The results of simulations to predict segregation from solidification and subsequent  
107 homogenization during a 1673K heat treatment for 35 h for NbTaTiW are shown in Figure 3.  
108 Figures 3(a), 3(b), and 3(c) simulate homogenization for a range of secondary dendrite arm  
109 spacings, with the 10 μm characteristic length scale resulting in almost complete removal of  
110 segregation. Similar behavior is shown in Figures 4(a), 4(b), and 4(c) for MoNbTaTi. The rate of  
111 homogenization is highly dependent on the length scale over which the solidification segregation

112 is observed. It can be seen that the as-cast condition for both alloys mostly follow the trends  
 113 predicted above; the dendrite cores are Mo, Ta, and W-rich, while the interdendritic regions are  
 114 Nb and Ti-rich.



115  
 116 Figure 3: Solidification and homogenization simulations (35 h, 1673K) of NbTaTiW for length  
 117 scales of (a) 1000  $\mu\text{m}$ , (b) 100  $\mu\text{m}$ , and (c) 10  $\mu\text{m}$ , where Scheil is the composition  
 118 profile from the Scheil calculation, HT is the composition profile from the simulated  
 119 homogenization heat treatment. The distance (x-axis) is measured from the center of  
 120 the secondary dendrite arm to the interdendritic region.  
 121



122

123 Figure 4: Solidification and homogenization simulations (35 h, 1673K) of MoNbTaTi for length  
124 scales of (a) 1000  $\mu\text{m}$ , (b) 100  $\mu\text{m}$ , and (c) 10  $\mu\text{m}$ , where Scheil is the composition  
125 profile from the Scheil calculation, HT is the composition profile from the simulated  
126 homogenization heat treatment. The distance (x-axis) is measured from the center of  
127 the secondary dendrite arm to the interdendritic region.

128

129 Experimental EDS measurements of the principal elements at the dendrite core and interdendritic  
130 regions taken in the as-cast condition are compared to the solidification simulation results in  
131 Tables 2 and 3. The simulation results captured in Table 2 are representative of the extremes,  
132 where the dendrite core composition is taken at a distance of zero and the interdendritic  
133 composition is taken at the maximum distance from the center of the dendrite. While Nb  
134 concentration in the dendrite core is similar in both the experimental and simulation data with a  
135 difference of only 0.6 at%, all other elements have compositional differences ranging from 5.4  
136 at% (Ta in the dendrite core) to 37.2 at% (Ti in the interdendritic region). This can be attributed  
137 to the error inherent in experimentally estimating the center of the dendrite core and  
138 interdendritic regions. If the measurements are instead assumed to be taken off-center, the  
139 solidification segregation simulation is in much better agreement, as shown in Table 3. These  
140 off-center measurements were assumed to be taken at 50% and 90% of the length-scale for the  
141 dendrite core and interdendritic regions, respectively. These locations were picked for two  
142 reasons: it is more difficult to measure the center of the dendrite core than the interdendritic  
143 region, and the composition within the dendrite core changes more gradually than the  
144 interdendritic region. Tables 4 and 5 show simulation results for dendrite cores and interdendritic  
145 regions at the various length scales and experimental EDS measurements after homogenization.  
146 Both tables include the assumption that the experimental measurements were not taken at the  
147 exact centers of the dendrite core and interdendritic region. The 1000  $\mu\text{m}$  length scale simulation  
148 data agrees the most with the experimental data for both RMPEAs, although this length scale is  
149 approximately two orders of magnitude greater than measured in Figures 1 and 2. For  
150 NbTaTiW, the 100  $\mu\text{m}$  simulation data remains close to the experimental data; the biggest  
151 discrepancy is observed for Ti, for which the simulation predicts it to be approximately 4 at%  
152 higher in the dendrite core than the experimental data exhibits. The 10  $\mu\text{m}$  simulation is the least  
153 accurate of the length scales, as it predicts almost full homogenization after heat treatment, while  
154 Figure 1(b) shows that segregation is still present. All but the concentration of Nb in the dendrite  
155 core are off by about 2 at% or more. For MoNbTaTi, the 100  $\mu\text{m}$  simulation predicts almost full

156 homogenization, with the simulation prediction for Ta at the dendrite core differing from the  
 157 experimental data by approximately 3 at%. The 10  $\mu\text{m}$  simulation displays the greatest deviation  
 158 from the experimental data, predicting complete homogenization, while Figure 2 shows that  
 159 segregation remains after heat treatment. While the sluggish diffusion effect was considered to  
 160 be a possible contributing factor in the discrepancy between the experimental results and the  
 161 simulations, recent studies suggest sluggish diffusion is caused by specific compositions and is  
 162 not a general HEA effect. [25,26]. It is more likely that DICTRA, with the mobility data in the  
 163 MOBHEA2 database predicts faster diffusion than the actual rate observed experimentally. The  
 164 simulation was successful, however, in predicting the segregation trends during solidification  
 165 and heat treatment.

166

167 Table 2: As cast compositional (at%) data for experimental and simulation solidification of  
 168 NbTaTiW, with simulated data taken from the extremes.

169

		<b>Nb</b>	<b>Ta</b>	<b>Ti</b>	<b>W</b>
<b>Dendrite Core</b>	<b>Experimental</b>	22.3	24.5	26.0	27.2
	<b>Simulated</b>	21.7	29.9	10.6	37.8
<b>Interdendritic</b>	<b>Experimental</b>	24.3	14.1	52.3	9.1
	<b>Simulated</b>	8.3	2.2	89.5	0.004

170

171 Table 3: As cast compositional (at%) data for experimental and simulation solidification of  
 172 NbTaTiW, including the assumption experimental measurements were taken at 50%  
 173 and 90% of the length-scale for the dendrite core and interdendritic region, respectively  
 174 instead of the exact center of the dendrite core and interdendritic region.

175

		<b>Nb</b>	<b>Ta</b>	<b>Ti</b>	<b>W</b>
<b>Dendrite “Core”</b>	<b>Experimental</b>	22.3	24.5	26.0	27.2
	<b>Simulated</b>	27.0	24.5	23.3	25.2
<b>Interdendritic</b>	<b>Experimental</b>	24.3	14.1	52.3	9.1
	<b>Simulated</b>	25.5	14.6	52.5	7.3

176

177 Table 4: Heat treated compositional (at%) data for experiments and simulations for NbTaTiW.

178

		<b>Nb</b>	<b>Ta</b>	<b>Ti</b>	<b>W</b>
<b>Dendrite Core</b>	<b>Experimental</b>	23.2	27.9	19.8	29.1
	<b>1000 <math>\mu\text{m}</math></b>	25.1	26.4	19.3	29.2
	<b>100 <math>\mu\text{m}</math></b>	23.5	24.8	23.8	27.9
	<b>10 <math>\mu\text{m}</math></b>	24.6	24.5	24.3	26.6

Interdendritic	Experimental		26.5	23.9	26.3	23.5
	Simulated	1000 $\mu\text{m}$	26.6	23.4	26.5	23.6
		100 $\mu\text{m}$	28.1	22.8	25.5	23.6
		10 $\mu\text{m}$	24.2	25.8	24.5	25.5

179  
180  
181

Table 5: Heat treated compositional (at %) data for experiments and simulations for MoNbTaTi.

		Mo	Nb	Ta	Ti	
Dendrite Core	Experimental	21.7	22.3	33.5	21.4	
	Simulated	1000 $\mu\text{m}$	23.7	22.4	30.5	23.4
		100 $\mu\text{m}$	22.4	23.4	29.3	24.9
		10 $\mu\text{m}$	21.4	23.4	29.3	25.9
Interdendritic	Experimental	22.8	24.5	25.5	28.4	
	Simulated	1000 $\mu\text{m}$	17.7	26.3	30.5	25.4
		100 $\mu\text{m}$	22.0	23.4	29.8	24.7
		10 $\mu\text{m}$	21.4	23.4	29.3	25.9

182

183 This discrepancy between the experimental and simulation results for homogenization of  
184 MoNbTaTi prompted additional exploration of diffusion behavior in refractory binary systems.  
185 Homogenization simulations were performed using DICTRA for the Mo/Nb, Nb/W, Ta/W, and  
186 Ti/W binary systems, for a heat treatment at 1400°C for 35 hours. The calculated compositional  
187 profiles from these simulations are shown in Figure 5 below. As a comparison, characteristic  
188 self-diffusion lengths for Mo, Nb, Ta, Ti and W and inter-diffusion lengths for Ta in Ta<sub>30</sub>W<sub>70</sub>  
189 and W in Ta<sub>30</sub>W<sub>70</sub> were calculated using Equation 1, shown below, with literature values for the  
190 self-diffusion and inter-diffusion coefficients as a function of temperature, [27,28]

$$L_D = \sqrt{D_0 e^{\left(\frac{-E}{RT}\right)} t} \quad \text{Equation 1}$$

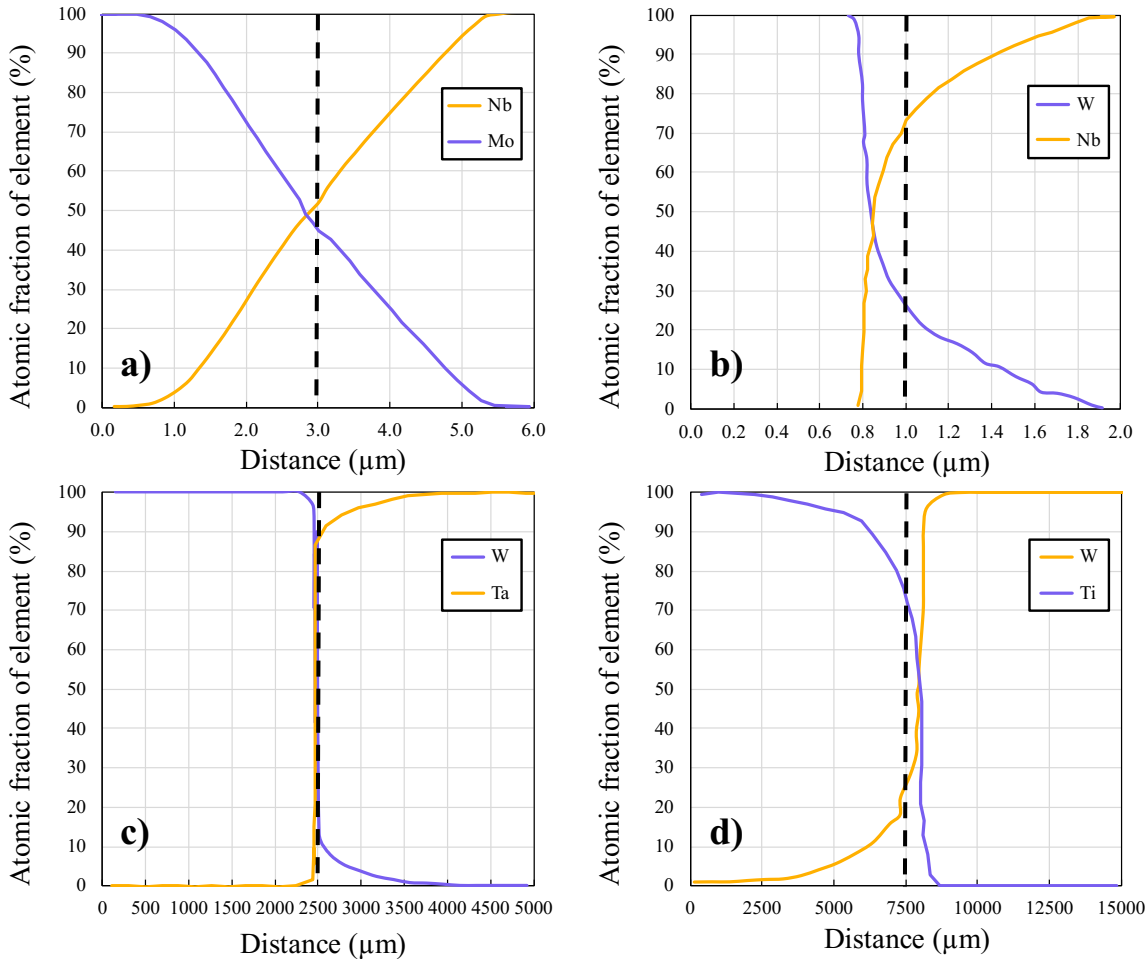
191 where  $L_D$  is the diffusion length,  $D_0$  is the diffusion coefficient, E is the activation energy for  
192 diffusion, R is the ideal gas constant, T is temperature, and t is time. Comparing the results from  
193 these two calculation methods, a discrepancy specific to the diffusivity of Ta was found.  
194

195 Table 6: Calculated self-diffusion and inter-diffusion lengths ( $L_D$ ) for a heat treatment for 35  
 196 hours at 1673K. The diffusion coefficient pre-factor, activation energies and relevant  
 197 temperature ranges for both values used to calculate the diffusion lengths are also  
 198 listed.

	$D_0 (10^{-4} \text{ m}^2\text{s}^{-1})$	$E (\text{kJ mol}^{-1})$	Applicable Temp Range (K)	$L_D (\mu\text{m})$
<b>Mo (max)</b>	8.0 <sup>a</sup>	488.2 <sup>a</sup>	1087-2500 <sup>a</sup>	0.24
<b>Mo (min)</b>	1.39 <sup>b</sup>	549.3 <sup>b</sup>	1363-2724 <sup>b</sup>	0.111
<b>Nb (max)</b>	1.1 <sup>a</sup>	401.9 <sup>a</sup>	1224-2668 <sup>a</sup>	2.0
<b>Nb (min)</b>	3.7 <sup>a</sup>	438.0 <sup>a</sup>	1354-2692 <sup>a</sup>	0.99
<b>Ta (max)</b>	0.124 <sup>a</sup>	413.2 <sup>a</sup>	1523-2576 <sup>a</sup>	0.443
<b>Ta (min)</b>	0.21 <sup>a</sup>	423.6 <sup>a</sup>	1261-2993 <sup>a</sup>	0.40
<b>Ti (max)</b>	$4.54 \times 10^{-4}$ <sup>a</sup>	131.0 <sup>a</sup>	1228-1784 <sup>a</sup>	682
<b>Ti (min)</b>	1.09 <sup>a</sup>	251.2 <sup>a</sup>	1172-1813 <sup>a</sup>	444
<b>W (max)</b>	0.04 <sup>a</sup>	525.8 <sup>a</sup>	1705-3409 <sup>a</sup>	0.004
<b>W (min)</b>	46 <sup>a</sup>	665.7 <sup>a</sup>	1705-3409 <sup>a</sup>	0.00098
<b>Ta in Ta<sub>30</sub>W<sub>70</sub></b>	1.8 <sup>b</sup>	553.9 <sup>b</sup>	1573-2373 <sup>b</sup>	0.011
<b>W in Ta<sub>30</sub>W<sub>70</sub></b>	0.17 <sup>b</sup>	510.8 <sup>b</sup>	1573-2373 <sup>b</sup>	0.016

200 <sup>a</sup>Ref. [27], <sup>b</sup>Ref. [28]

201  
 202 The simulation (Figure 5(c)) predicts the TaW diffusion couple diffuses about 100  $\mu\text{m}$  (measured  
 203 at 25 at%), while the calculated characteristic diffusion length only predicts diffusion of less than  
 204 0.1  $\mu\text{m}$ . It is recognized that the interdiffusion coefficient for the relevant binary system, which  
 205 depends upon composition, is necessary to perform a homogenization simulation. Unfortunately,  
 206 the availability of interdiffusion data is more limited than self-diffusion data, which is why only  
 207 two interdiffusion calculations were performed to verify order of magnitude. Given the only  
 208 interdiffusion coefficients used were that of Ta and W in Ta<sub>30</sub>W<sub>70</sub>, the discrepancy between the  
 209 simulated TaW diffusion couple and the calculations remains.



211  
 212  
 213 Figure 5: Diffusion couple simulations of (a) MoNb, (b) NbW, (c) TaW, and (d) TiW after a heat  
 214 treatment of 35 hours at 1673K. The original interface position is shown with a black  
 215 dashed line.  
 216

217 The predicted solidification segregation from the Scheil-Gulliver model using compared well  
 218 with the experimental data. However, the homogenization simulations using DICTRA did not  
 219 agree with the experimental data, predicting homogenization to occur in much shorter times than  
 220 was actually observed. After analyzing the diffusion couple simulation results, it can be  
 221 hypothesized that the faster than experimentally observed homogenization of the two RMPEAs  
 222 studied can be attributed to the diffusivity of Ta within the MOBHEA2 database. The rest of the  
 223 diffusion couple results agree with the rough diffusion calculations, suggesting DICTRA would  
 224 be accurate in simulating RMPEA alloys without Ta. That said, the simulations are valuable to  
 225 show qualitative trends. As the length scale of the solidification segregation decreases, the  
 226 simulations predict the degree of homogeneity to increase, given a heat-treatment at 1673K for

227 35 h. This trend agrees with theory, when assuming the concentration of each element varies  
228 sinusoidally with distance in one dimension. The simulation is being performed over half a  
229 period, starting at either the maximum or minimum, depending on the element. The amplitude  
230 ( $\beta$ ) of the concentration profile after a time (t) is given by the following equation:

$$231 \quad \beta = \beta_0 \exp \frac{-t\pi^2 D_B}{l^2} \quad \text{Equation 2}$$

232 where  $\beta_0$  is the amplitude at  $t = 0$ ,  $D_B$  is the diffusion coefficient of the element in question, and  
233  $l$  is the length scale. [29]. This equation shows that decreasing the length scale, while keeping all  
234 else constant, will decrease the amplitude, which is exactly what the simulations predict.

235

236 In summary, due in large part to the high melting temperatures of refractory metals and the  
237 challenges associated with obtaining experimental data, opportunity exists to continually  
238 improve available thermodynamic databases, particularly for refractory alloys and RMPEAs.  
239 Research in this area is largely guided by simulations performed using computational  
240 thermodynamic and kinetic software. Therefore, the generation of both thermodynamic and  
241 kinetic data to fill in the current knowledge gaps will be essential to advancing the state of the art  
242 in refractory alloy and heat treatment design.

243

244 The need for structural metallic alloys for use in ultrahigh temperature applications has led to the  
245 exploration of RMPEAs, largely through a combination of simulation and experiments.  
246 Simulations were performed using the Scheil-Gulliver model and DICTRA in Thermo-Calc® to  
247 predict solidification segregation and homogenization in two RMPEA alloys, namely NbTaTiW  
248 and MoNbTaTi. While the Scheil-Gulliver model can accurately predict the solidification  
249 segregation of the RMPEAs, DICTRA does not predict the extent of homogenization observed  
250 experimentally when realistic length scales are used for a 35 h, 1673K heat treatment. The  
251 homogenization heat treatments performed with realistic length scales predict homogenization to  
252 occur faster than the experimental data shows. In particular, these results suggest the diffusivity  
253 of Ta in the MOBHEA2 database may be too high. Despite some discrepancies between  
254 simulation and experiment, DICTRA predicts minimum homogenization times that can be  
255 explored by heat treatment, thereby accelerating the design of future experiments to assess the  
256 thermodynamics and kinetics of RMPEAs. Future work can include comparing the RMPEA

257 simulations with relevant binary simulations to further distinguish inconsistencies in either the  
258 database or experimental data.

259

260 **Acknowledgements**

261 This work was funded by the Department of Energy's Kansas City National Security Campus  
262 which is operated and managed by Honeywell Federal Manufacturing Technologies, LLC under  
263 contract number DE-NA0002839. The electron microscopy and the contributions of author F.G.  
264 Coury were separately supported by the Center for Advanced Non-Ferrous Structural Alloys  
265 (CANFSA), a National Science Foundation Industry/University Cooperative Research Center  
266 (I/UCRC) [Award No. 1624836] at the Colorado School of Mines and the Conselho Nacional de  
267 Desenvolvimento Científico e Tecnológico - Brasil (CNPq) [Grant No. 424645/2018-1]. We also  
268 thank ATI for producing the experimental alloys studied here.

269 **Conflict of Interest statement**

270 On behalf of all authors, the corresponding author states that there is no conflict of interest.

271 **References**

272 1. O. N. Senkov, D. B. Miracle, K. J. Chaput, and J.-P. Couzinie, *J. Mater. Res.* **33**, 3092 (2018).  
273 2. M.-H. Tsai and J.-W. Yeh, *Materials Research Letters* **2**, 107 (2014).  
274 3. J. Chen, X. Zhou, W. Wang, B. Liu, Y. Lv, W. Yang, D. Xu, and Y. Liu, *Journal of Alloys and Compounds* **760**, 15 (2018).  
275 4. O. N. Senkov, C. Zhang, A. L. Pilchak, E. J. Payton, C. Woodward, and F. Zhang, *Journal of Alloys and Compounds* **783**, 729 (2019).  
276 5. S. Praveen and H. S. Kim, *Advanced Engineering Materials* **20**, 1700645 (2017).  
277 6. J.-P. Couzinié, O. N. Senkov, D. B. Miracle, and G. Dirras, *Data in Brief* **21**, 1622 (2018).  
278 7. A. B. Melnick and V. K. Soolshenko, *Journal of Alloys and Compounds* **694**, 223 (2017).  
279 8. F. G. Coury, M. Kaufman, and A. J. Clarke, *Acta Materialia* **175**, 66 (2019).  
280 9. F. Maresca and W. A. Curtin, *Acta Materialia* **182**, 235 (2020).  
281 10. F. G. Coury, T. Butler, K. Chaput, A. Saville, J. Copley, J. Foltz, P. Mason, K. Clarke, M. Kaufman, and A. Clarke, *Materials & Design* **155**, 244 (2018).  
282 11. U. E. Klotz, C. Solenthaler, and P. J. Uggowitzer, *Materials Science and Engineering: A* **476**, 186 (2008).  
283 12. T. Yamashita, K. Okuda, and T. Obara, *Journal of Phase Equilibria* **20**, 231 (1999).  
284 13. V. Knežević, J. Balun, G. Sauthoff, G. Inden, and A. Schneider, *Materials Science and Engineering: A* **477**, 334 (2008).  
285 14. A. W. Zhu, B. M. Gable, G. J. Shiflet, and E. A. Starke, *Advanced Engineering Materials* **4**, 839 (2002).  
286 15. H.-L. Chen, Q. Chen, and A. Engström, *Calphad* **62**, 154 (2018).  
287 16. P. D. Jablonski and J. A. Hawk, *Journal of Materials Engineering and Performance* **26**, 4 (2017).  
288 17. P. L. Conway, T. P. C. Klaver, J. Steggo, and E. Ghassemali, *Materials Science and Engineering: A* **830**, 142297 (2022).  
289 18. M. Asadikiya, Y. Zhang, L. Wang, D. Apelian, and Y. Zhong, *Journal of Alloys and Compounds* **891**, 161836 (2022).  
290 19. G. H. Gulliver, *J Inst Met* **13**, 263 (1915).  
291 20. E. Scheil, *International Journal of Materials Research* **34**, 70 (1942).  
292 21. A. Borgenstam, L. Höglund, J. Ågren, and A. Engström, *Journal of Phase Equilibria* **21**, 269 (2000).  
293 22. F. G. Coury, *Solid Solution Strengthening Mechanisms in High Entropy Alloys*, Dissertation, Colorado School of Mines, 2018.  
294 23. H. W. Yao, J. W. Qiao, M. C. Gao, J. A. Hawk, S. G. Ma, H. F. Zhou, and Y. Zhang, *Materials Science and Engineering: A* **674**, 203 (2016).  
295 24. H. Yao, J.-W. Qiao, M. C. Gao, J. A. Hawk, S.-G. Ma, and H. Zhou, *Entropy* **18**, 189 (2016).  
296 25. J. Dąbrowa, M. Zajusz, W. Kucza, G. Cieślak, K. Berent, T. Czeppe, T. Kulik, and M. Danielewski, *Journal of Alloys and Compounds* **783**, 193 (2019).  
297 26. W. Kucza, J. Dąbrowa, G. Cieślak, K. Berent, T. Kulik, and M. Danielewski, *Journal of Alloys and Compounds* **731**, 920 (2018).  
298 27. H. Mehrer, N. Stolica, and N. A. Stolwijk, *Landolt-Börnstein - Group III Condensed Matter* **64** (n.d.).  
299 28. W. F. Gale and T. C. Totemeier, *Smithells Metals Reference Book* (Elsevier, 2003).  
300 29. D. A. Porter and K. E. Easterling, *Phase Transformations in Metals and Alloys (Revised Reprint)* (CRC press, 2009).

317

318

319